658

TECHNICAL MEMORANDUM

On the dependence of ENSO simulation on the coupled model mean state

L. Magnusson, M. Alonso-Balmaseda and F. Molteni

Research Department

December 2011

Abstract

Systematic model error has been and remains a difficult problem for seasonal forecasting and climate predictions. An error in the mean state could affect the variability of the system. In this report, we investigate the impact of the mean state on the properties of ENSO. A set of long coupled integrations have been conducted, where the mean state has been modified by applying different flux correction schemes. It is shown that correcting the mean state improves the amplitude of SST inter-annual variability, the penetration of the ENSO signal into the troposphere and the spatial distribution of the ENSO teleconnections. An analysis of a multivariate PDF of ENSO shows clearly that the flux correction affects the mean, variance, skewness and tails of the distribution. The changes in the tails of the distribution are particularly noticeable in the case of precipitation, showing that without the flux correction the model is unable to reproduce the frequency of large events.

These results suggest that the current practice of removing the forecast bias a-posteriori is by no means optimal, since it can not deal with the strong nonlinear interactions. A consequence of this results is that the predictability on annual time-ranges could be higher than currently achieved. Whether or not the correction of the model mean state by some sort of flux-correction leads to better forecasts needs to be addressed. In anycase, flux correction may be a powerful tool for diagnosing coupled model errors and predictability studies.

1   Introduction

Systematic model error is a difficult problem for seasonal forecasting and climate predictions. Systematic model error means that the climatology of the model is different from the observed climatology, in the sense of the mean climate (the mean of a variable over a long period) and/or the variability around the mean state. In a nonlinear system, the different moments of the climatology are linked, and errors in the mean state could affect the variability of the system. In this report we will investigate the effect of the mean state focusing on the simulation and forecast of El Niño- Southern Oscillation (ENSO) related variability.

ENSO is the strongest known mode of the inter-annual variability in the climate system. Primarily affecting the sea-surface temperature in the mid and eastern equatorial Pacific, it has an impact on the atmospheric circulation on a global scale. Therefore it is crucial that a forecasting model for seasonal time-scales can simulate the behaviour of the phenomena. For climate predictions it is important for models to simulate the ENSO in order to capture the internal variability of the climate system and a possible change in variability due to increased greenhouse gas concentrations in the atmosphere.

The systematic error of coupled models in the tropical Pacific has been discussed extensively in the literature. Different models show different types of errors. The most common in coupled models consist of a warm bias off the eastern coast, attributed to the lack of upwelling and deficient representation of stratocumulus clouds; a cold bias associated with the cold tongue (either due to intensity error or geographical location error); the so-called double ITCZ, characterised by a too meridionally symmetric precipitation pattern, and the deficient representation of the intraseasonal oscillation. Several studies have argued that both errors in the mean and intraseasonal variability can affect the representation of ENSO (Kessler and Kleeman, 2000; Vitart et al., 2003; Lengaigne et al., 2004; Eisenman and Tziperman, 2005; Balmaseda and Anderson, 2009; Guilyardi et al., 2009). The interaction between model mean state and variability has been discussed in e.g Jin et al. (2008), Manganello and Huang (2009) and Spencer et al. (2007). While Jin et al. (2008) discuss the issue in the context of different models, Manganello and Huang (2009) discuss it in the context of the use of flux correction.

Although flux correction was widely used when coupled GCMs were first run, it has been considered

"taboo" by the scientific community since Neelin and Dijkstra (1995) argued that flux corrections could lead to non-natural variability patterns by disturbing the feedbacks operating in a free dynamical system. Indeed, flux correction should be avoided if the aim is the study of coupled feedbacks, and can be misleading for model development. In this study, we approach the problem from a very pragmatic point of view: can flux correction improve the forecasts?

The most common practice to deal with model error in seasonal forecasts is the a-posteriori removal of the model bias, which assumes that the error in the mean state does not interact with the inter-annual variability. Under this assumption, the bias is relatively easy to estimate and correct a-posteriori. With a feasible number of cases it is possible to obtain robust estimations of the bias as a function of the starting calendar month and lead time. However, a-posteriori correction of the variability is more difficult, and robust estimation requires larger number of samples. The assumption of linearity may hold in some systems at early forecast lead times, when the errors in the mean are not large enough. However, Balmaseda and Anderson (2009) argue that errors in the mean state of the coupled model are a serious obstacle to further improvements of seasonal forecasts. The a-posteriori correction is expected to be suboptimal for decadal forecasts, where the errors in the mean are well developed, and often beyond the threshold of nonlinear interactions.

In this study we use flux correction to exemplify the interaction between mean state errors and variability using a version of the ECMWF coupled model. The correction will be applied both to the heat and momentum fluxes. We investigate the effect of changing the mean state on the ENSO variability. The flux corrected experiments will be compared to a set of reference simulations that do not use any flux correction. We use the ECMWF seasonal forecast system but run the model with extended forecasts lengths. The focus will be on the tropical Pacific and the ability to model the ENSO variability. We will put this discussion in the context of the different forecast strategies. The results from this study should not be seen as universal but dependent on the flavour of the systematic error in the current model. The focus of this report is the ability to model the variability. An upcoming report will discuss the predictability and the ability to forecast specific events.

2 El Niño - Southern oscillation

ENSO is an inter-annual variability pattern in the tropical Pacific that affects the circulation in both the oceans and the atmosphere. An El Niño event (positive ENSO phase) appears as warming of the sea-surface temperature in the mid and eastern basin of the equatorial Pacific. The opposite is the La Niña that appears as anomalous cold SST in the same area.

The atmospheric counterpart of the El Niño oscillation is the Southern Oscillation (Walker, 1924), and it is related to fluctuations in the Walker circulation. The Walker circulation is a thermal circulation with easterly winds at surface, ascending motion over the Pacific warm-pool, westerly winds at the top of the troposphere and decending motions over the eastern Pacific. The strength of the Walker circulation can be measured by the sea-level pressure difference between the eastern and western part of the basin, and this is the basis for the Southern Oscillation Index (SOI). The SOI also reflects the strength of the trade winds over the Pacific.

The building up of an El Niño event can be explained by Bjerknes positive ocean-atmosphere feedback process (Bjerknes, 1969). The feedback process consists in the following steps: (1) a positive SST anomaly in the eastern Pacific (2) reduces the SST gradient in the basin. The reduced SST gradient in the basin leads to (3) an reduced Walker circulation, which (4) gives weaker trade winds. The trade winds drives the ocean circulation and weaker winds gives (5) rise a reduced upwelling of cold water in the

eastern part of the basin, which (1) strengthen the positive SST anomaly in the eastern part of the basin. To initialise the feedback loop it is believed that a sudden break in the easterly trade wind (westerly wind burst) allows a surge of warm water to propagate as a Kelvin wave towards the east, although this is also possible by the so-called delayed Oscillator mechanism (Suarez and Schopf, 1988), without invoking changes in the wind.

In order to break the positive feedback several mechanisms have been proposed: wave reflection at the ocean western boundary, a discharge process due to Sverdrup transport (Jin, 1997a), a western Pacific wind-forced Kelvin wave of opposite sign and anomalous zonal advection [all discussed in detail in Wang and Picaut (2004)]. After the culmination of the El Niño event the feedback loop is reversed and leads usually to anomalous cold SST (La Niña).

On the seasonal time-scale, predictability of ENSO is present in the forecasts. The El Niño has teleconnections to other parts of the atmospheric system and is therefore a key component in producing global seasonal forecasts. The teleconnections of ENSO are discussed in e.g. Ropelewski and Halpert (1987) and Halpert and Ropelewski (1992).

Not all El Niño events have the same structure. There is a variability on the longitudinal positioning of the maximum temperature and also in the development of the events. A presence of a decadal variability of the strength and positioning of the ENSO has been discussed in the literature [see e.g Balmaseda et al. (1995) and Kirtman and Schopf (1998)]. Decadal variability in the ocean could lead to changes in the predictability of ENSO.

In order to evaluate the ENSO, the average SST for different areas are commonly used. In this study we will refer to Niño3 (150°W-90°W,5°N-5°S) in the eastern part of tropical Pacific; Niño3.4 (170°W-120°W,5°N-5°S) in the central part and Niño4 (160°E-150°W,5°N-5°S) in the central-western part of the basin.

3 Reference data and model and experimental setup

3.1 Model

The model used for this study is the ECMWF IFS model (version 36r1) coupled with the NEMO ocean model version 3.0 (Madec, 2008). The resolution for the experiments is in the atmosphere T159 (which corresponds to an horizontal resolution of 150 km) and 91 vertical levels. For the ocean the ORCA1 grid is used, which has a 1 degree horizontal resolution with meridional refinements in the tropics. Instead of using a dynamical sea-ice model, the sea-ice is randomly sampled from historical data. The sea-ice is randomly selected from any of the 5 years before the simulation year, for details see Molteni et al. (2011). The perturbations for the ensemble members are generated by initial perturbation in the atmosphere (singular vectors) as well as using the SPPT scheme in order to simulate model uncertainties in the atmosphere (Palmer et al., 2009). The model runs include increased greenhouse gases following observed values. Variability of aerosols are not included in the model, leading to no effect of volcanic eruptions (except for the impact on greenhouse gases).

3.2 Experiments

Table 1 shows a summary of the experiments that have been undertaken. Decadal (10-year) forecasts have been initialised every fifth year with the first started in November 1965 and the last in November 2010. As

Name	Fc months	Members	Initialisation	Flux correction	Initial dates
Control	300	3	Full	None	3
StrongRelax	300	3	Full	None	3
WeakRelax	300	3	Full	Momentum	3
NOcorr	120	7	Anomaly	None	10
Ucorr	120	3	Full	Momentum	10
UHcorr	120	7	Full	Heat and Momentum	10

Table 1: Experiments

initial conditions for the atmosphere, the ERA-40 and after 1989, ERA Interim reanalysis have been used (Uppala et al., 2005; Dee et al., 2011). The ocean initial conditions are from the NEMOVAR-COMBINE (Balmaseda et al., 2010) ocean reanalysis. The ocean reanalysis uses fluxes from the ERA-reanalysis as well as sub-surface observations.

To obtain an estimate of the model climate, 3-member ensembles initialised in 1965, 1975 and 1985 have been run for 25 years (referred to as Control in what follows). These simulations are used to calculate the model climate for the anomaly initialisation (see below), as well as for diagnostics. An additional set of 25-year forecasts was conducted where the SST were strongly constrained to observations by a relaxation technique. This methodology has been used by Keenlyside et al. (2008) and Balmaseda and Anderson (2009) among others, to initialise coupled models. The resulting atmospheric fields are equivalent to those obtained by AMIP integrations (Atmospheric only simulation forced by observed SST). Results from this experiment will be used for the calculation of the momentum flux correction. The SST data used for the relaxation is the same as for ERA-40 up to 1981 and after that Reynolds version 2 (Reynolds et al., 2002).

3.3 Reference Climate

As a reference climatology for the ocean, the NEMOVAR-COMBINE reanalysis will be used, which is available for the period 1958-2009. For the atmospheric diagnostics, we will mainly limit the evaluation to the ERA Interim period (1979-2010). For the precipitation climatology, data from Global Precipitation Climatology Project GPCP version 2 (Huffman et al., 2009) will be used as well as ERA Interim.

3.4 Model climate

Figure 1 shows the bias in the 2-metre temperature from the 25-year control simulations. The model climate has been computed by aggregating together year 14-24 from from each of the three control simulations, which in total cover the period 1979-2008: 1979-1988 from the forecast initialised in 1965, 1989-1998 for the forecast initialised in 1975 and 1999-2008 from the forecast initialised in 1985. The bias has been calculated with respect to the ERA Interim reanalysis between 1979 and 2008. In general, the model is too cold with a global bias of 1.8 Kelvin. The cold bias is present all over the tropics and extra-tropics, while the Southern Ocean exhibits a warm bias. The structure of the bias leads to a weakening of the meridional temperature gradient.

Figure 2(a) shows the bias in the zonal component of the 10-metre wind speed for the long control simulation, calculated for the same period as the 2-metre temperature bias. Generally, the bias is less than 1 m/s, with a few exceptions. In the Southern Ocean the westerlies are reduced over the southern
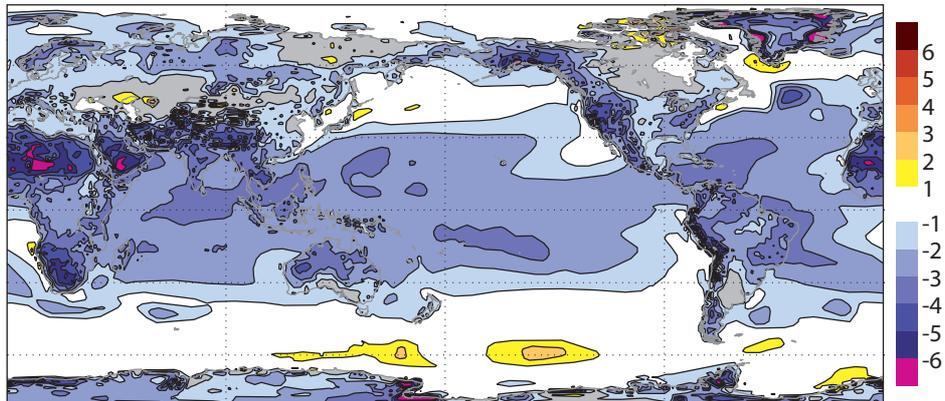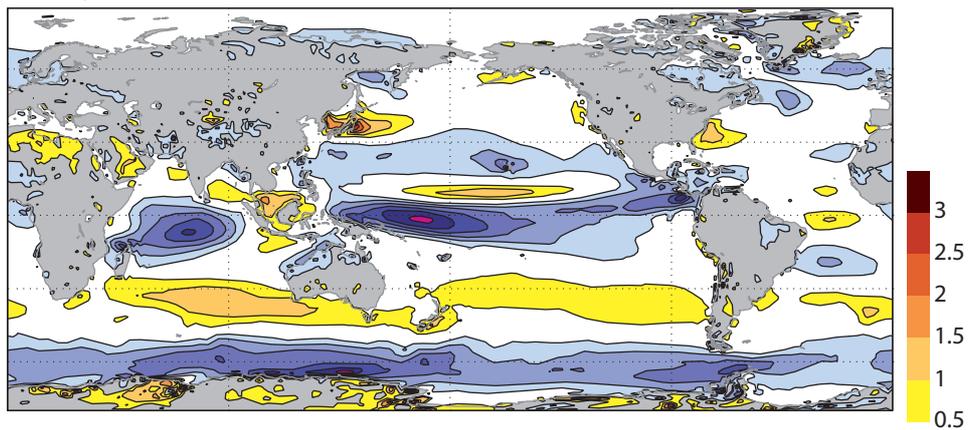
Figure 1: Bias in 2-metre temperature for the long control simulation, forecast year 14-24.

a) Coupled model

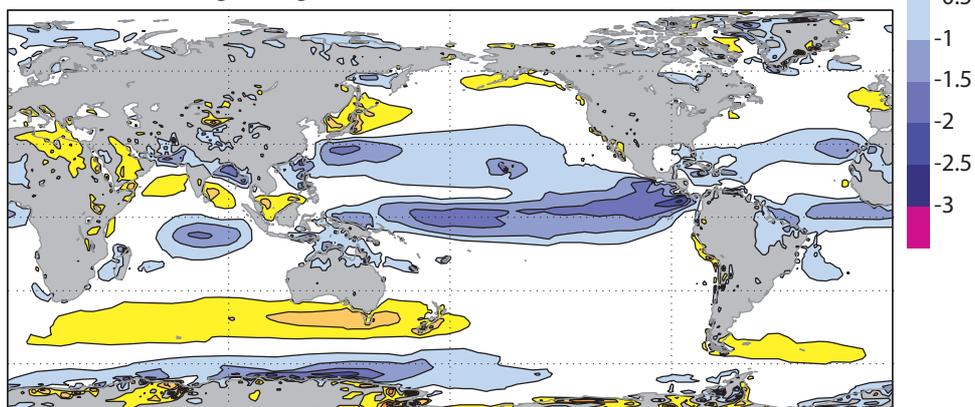**b)** Simulation using strong SST relaxation

Figure 2: Bias in zonal 10-metre wind. Forecast year 14-24.

edge of Antarctic Circumpolar Current. The largest bias appears in the western tropical Pacific, with values of up to 3 m/s. The bias is of the same order of magnitude as the wind speed in the reanalysis, meaning that the wind speed in the model is about twice the reanalysis value. As discussed in Section 2, the zonal wind in the western tropical Pacific has a large influence on the ENSO, and it also impacts the state of the thermocline and SST.

Figure 2(b) shows the same as Figure 2(a) but for the experiment using a strong relaxation to the observed SST. By constraining the SSTs, the wind bias is reduced in the Equatorial Pacific and Indian Ocean. The impact of SST is especially large in the western part of the basin where the bias is reduced by 50%. This illustrates clearly the positive feedback between SST and wind bias in the coupled model. It also shows that the atmospheric model has a strong wind bias, per se. The error in the wind over most of the Antarctic circumpolar Current seems to be of oceanic origin, since it largely disappears when the atmosphere is forced by observed SST (except for the cyclonic feature south and east of Australia).

3.5   Flux correction

Model improvement is the ultimate way of reducing model biases. As a temporary solution until the problems in the model are detected and solved, one could compensate for the systematic errors by applying empirical corrections. One specific correction is the so-called flux correction, applied only in the coupling between the atmosphere and the ocean. The use of flux-correction has recently been discussed in Spencer et al. (2007) and Manganello and Huang (2009). In the experiments presented here, the flux correction is applied on the fields passed from the atmospheric model to the ocean model. In order to represent the seasonal cycle of the systematic errors, correction fields have been estimated for each calendar month. The monthly flux correction climatology is then linearly interpolated in time before applying to the coupling interface for a given day.

One could expect that errors originate both from the heat flux to the ocean and the momentum flux. As seen in the previous section [Figure 2(a) and Figure 2(b)], a wind bias is present but could be reduced by correcting the SST bias. However, the SST bias could be reduced by reducing the wind bias. Therefore a strategy for correcting both components has been applied. The flux correction has been calculated in two steps. Firstly, the strong SST relaxation simulations have been used in order to calculate the wind bias if the SST is unbiased [see Figure 2(b)]. The momentum flux correction has been estimated from the two 25-year simulations starting in 1965 and 1975 (3-member ensembles), by comparing the surface stresses in the forecasts with the reanalysis data. The first 5 years of each simulation have not been used in order to let the atmospheric model drift. As a second step, a similar set of forecasts has been run using the momentum-flux correction and a weak SST-relaxation (40W/K), in order to calculate the required heat-flux correction with the applied momentum flux correction. This strategy yields a heat-flux correction suitable to be used together with momentum-flux correction and that partly accounts for the feedback effects.

In what follows, we refer to Ucorr as the forecast using momentum-flux correction only (both on u and v components), and to UHcorr as the forecasts using both momentum and heat-flux correction.

Figure 3(a) shows the monthly dependence of the zonal component momentum-flux correction for the Niño4 area, located in the western part of the tropical Pacific. Here we see a minimum in April and a maximum in July-August when the strongest upwelling takes place. The correction is generally positive (towards westerly stresses) in order to reduce the too strong easterlies.

Figure 3(b) shows the heat-flux correction required when the momentum flux correction is applied, as a function of calendar month for the Niño3 area, which is located in the eastern part of the Tropical Pacific
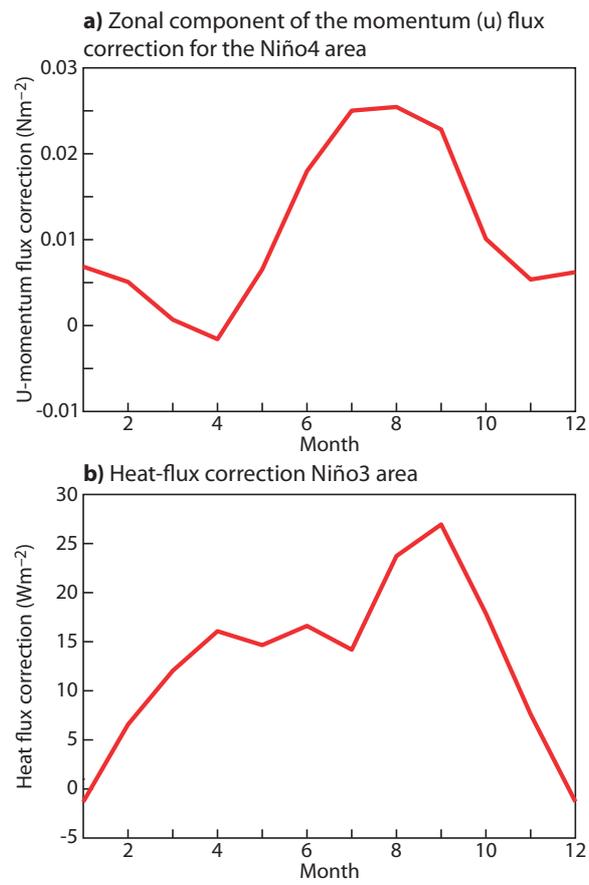
Figure 3: *Flux correction as a function of calendar month.*

were the cold tongue is present and where we have the strongest bias in SST. A positive correction means that heat is added to the ocean. We see in the figure that we have a seasonal variation of the required heat-flux correction. A maximum appears in September while the correction is close to 0 (or even negative) in January.

3.6   Reference simulation

Due to the difference in mean climate between the analysis (our best estimate of the truth) and the model, a forecast initialised from an analysis will drift torwards the model climate. A large part of the model drift can be avoided by initialising the model on its own attractor (here we define the attractor as the phase space where the model/nature evolves). This technique is referred to as anomaly initialisation and is used in several studies e.g. Schneider et al. (1999), Pierce et al. (2004) and Smith et al. (2007). In this study we use anomaly initialisation for the reference simulations in order to reach the model climate more quickly, without needing to throw away a lot of data during the model drift.

For the initialisation, the observed anomalies (full 3-dimensional ocean field) is added to the model climate. The model climate is estimated from the 25-years control integrations, where the first 10 years of the simulations are not used in order to let the model drift to its own climatology. The climatology of the analysis has been calculated from the ocean reanalysis, spanning the same time period used in the estimation of the model climate. This period is chosen so that the difference between the climatologies is calculated with the same change of greenhouse gases for the both. The model and analysis climate is calculated for the actual date for initialisation.

The reference forecasts using anomaly initialisation will be referred to as NOcorr.

4   Results

Figure 4 shows examples of SST forecasts for Niño3.4 with year 2-4 plotted from one initial date (November 1995), in order to illustrate the differences between forecasts with and without flux-correction. We see a clear difference between the UHcorr, Ucorr and NOcorr in terms of both mean state and variability. In this section we show the results from the different experiments in the form of mean climate, inter-annual variability, multi-variate ocean variability and effects on the atmospheric variability. All results here has a focus on the Niño3.4 region, situated in the middle of the Tropical Pacific.

4.1   Mean climate

Figure 5 shows the mean SST [Figure 5(a)] for the tropical Pacific and a cross-section of the mean temperature along the equator [Figure 5(b)]. At the surface, we find the highest temperatures in the western part of the basin, with temperatures up to 30°C. Further east the temperature is colder due to upwelling of cold water. Studying the cross-section, we see that the warm pool extends vertically in the west, while the 20°C isoterm almost reaches the surface in the east.

Figure 6 shows the difference in SST between the NOcorr forecast and the reanalysis, yielding a measure of the model bias. The forecast data is averaged over forecast years 3-10 and one initial date (1980), and the bias is calculated in respect to the analysis climate shown in Figure 5. Generally for the tropical Pacific, we find a strong cold bias, which has its maximum along the equator. At its maximum, the bias reaches 2.5 Kelvin. Figure 6(b) shows a vertical cross section of the temperature bias along the equator
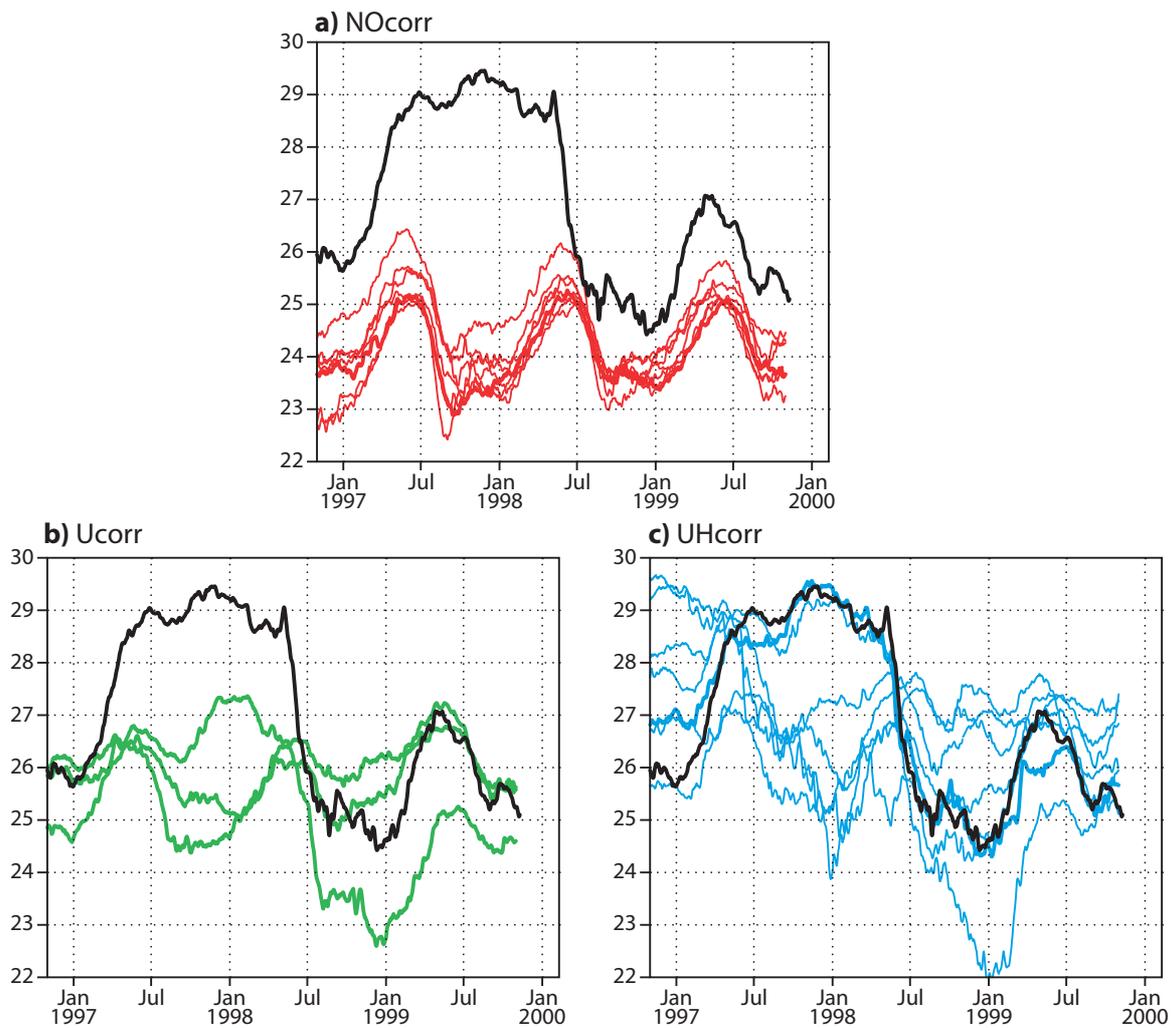
Figure 4: SST forecast for Niño3.4, year 2-4 from decadal forecasts initialised in November 1995 (coloured lines) and the reanalysis (black). For NOcorr and UHcorr the member that will serve a example forecast is highlighted (thick lines).
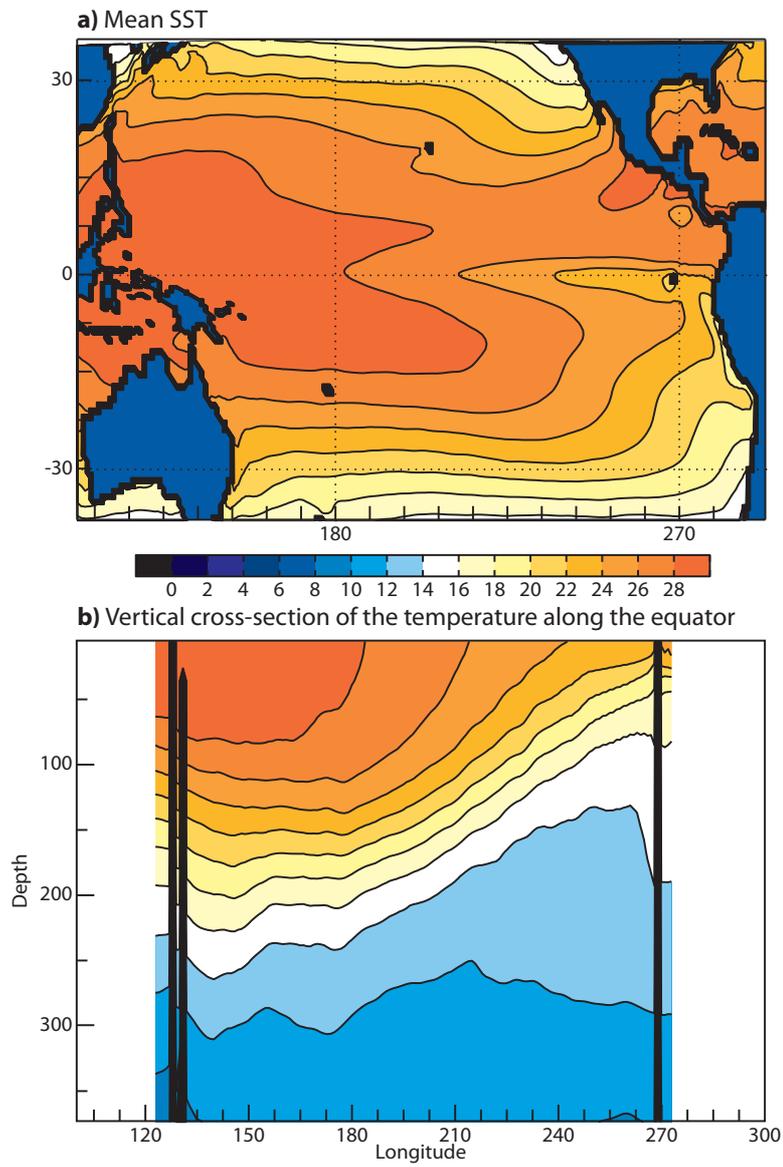
a) Mean SST

b) Vertical cross-section of the temperature along the equator

Figure 5: Mean of the reanalysis for 1983 to 1990.

a) SST bias

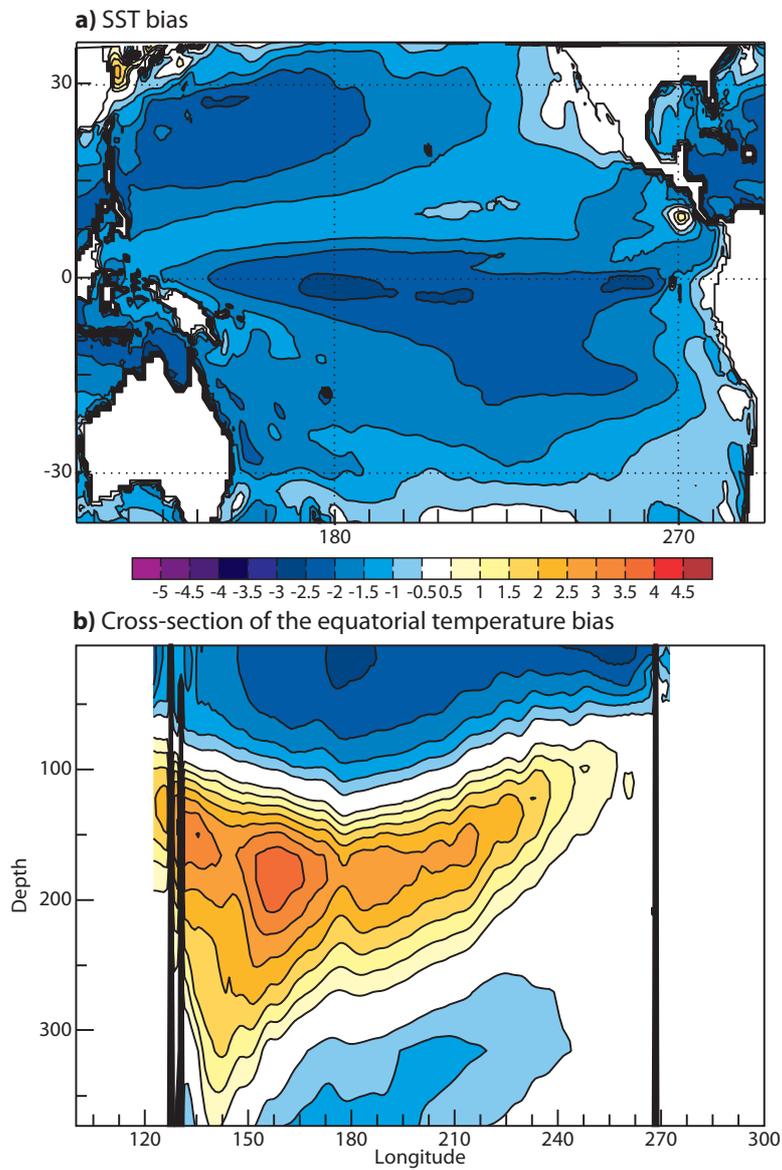**b)** Cross-section of the equatorial temperature bias

Figure 6: Difference between the NOcorr forecast and the reanalysis for forecast year 3-10 (initial date November 1980).

in the Pacific for the same data as shown in Figure 6(a). As expected from the SST bias plot, a cold bias is present at the surface. On other hand we find a warm bias between 100-300 metres, which is strongest in the western part of the basin. This dipole structure indicates that the bias is due to an overly strong equatorial circulation (too strong upwelling in the east and a too strong downwelling in the west).

Figure 7 shows the same as Figure 6 but for the Ucorr experiment. For the SST bias [Figure 7(a)], the momentum-flux correction is able to reduce the cold bias in the tropical Pacific, which indicates that the tropical bias is connected to the wind stress. Figure 7(b) show the vertical cross-section of the ocean temperature bias for the Ucorr experiment. Comparing with the NOcorr forecast [Figure 6(b)], the dipole bias structure is strongly reduced by using momentum-flux corrections, which may be explained by the fact that the flux correction reduces the easterly wind-stress and slows down the equatorial ocean circulation. However, there is still a bias present at the surface, and a warming of the thermocline, consistent with the too diffuse thermocline, which is a characteristic of this version of the NEMO model and observed in ocean only runs (not shown).

When using both momentum and heat-flux correction [Figure 8(a)], the SST bias is strongly reduced, which is the objective of the heat flux correction. Figure 8(b) shows the vertical cross-section of the bias for the UHcorr experiment. Comparing with the Ucorr experiment [Figure 7(b)], the cold bias in the thermocline is further reduced in the west by the use of the heat-flux correction. The warming along the thermocline is increased, especially in the eastern part. This behaviour is consistent with the heat flux correction partially compensating for errors in the upper ocean vertical mixing.

Figure 9 shows the monthly mean SST for Niño3.4 for the different experiments averaged over all initial dates and forecast year 5 to 10. The NOcorr experiment (red) exhibits a cold bias and a seasonal cycle that is too strong compared to the reanalysis (black). The stronger seasonal cycle is mainly due to the strong cold bias in September (the same period as the flux correction is at its strongest). Another feature is the slight shift in the maximum of the seasonal cycle, by about one month for NOcorr compared to the reanalysis. This pronounced bias is reduced by the momentum flux correction (green), which has a similar amplitude on the seasonal cycle as the reanalysis. The improvement using momentum flux correction during the boreal autumn is logical because the flux correction is strongest during that period. For the UHcorr experiment, the bias is less than 0.5 Kelvin for all months.

4.2 Inter-annual variability

An important aspect of the ENSO simulation is the simulated amplitude of the SST anomalies. In Guilyardi et al. (2009), the SST variability of several climate models is compared and a large diversity is found in the tropical Pacific, both regarding amplitude and location of the variability.

Figure 10 shows the inter-annual variability of the Niño3.4 SST as a function of calendar month. The forecast data used is for the initial dates 1965 to 2000 and forecast year 5 to 10. The reanalysis data is from 1970 to 2010. The inter-annual variability is calculated as the standard deviation with the seasonal cycle removed. For the reanalysis, means for 1970-1980 (dotted) and 1990-2000 (dashed) have also been plotted.

The general feature in the results is that the NOcorr experiment yields the lowest variability, much lower than the reanalysis. On contrary, the UHcorr yields a much higher variability than the NOcorr experiment and also higher than the reanalysis. The Ucorr experiment is in between and closest to the reanalysis, albeit underestimating the variability during the boreal winter. Our results are in line with Guilyardi (2006), in that models with strong seasonal cycle have a weak ENSO amplitude.
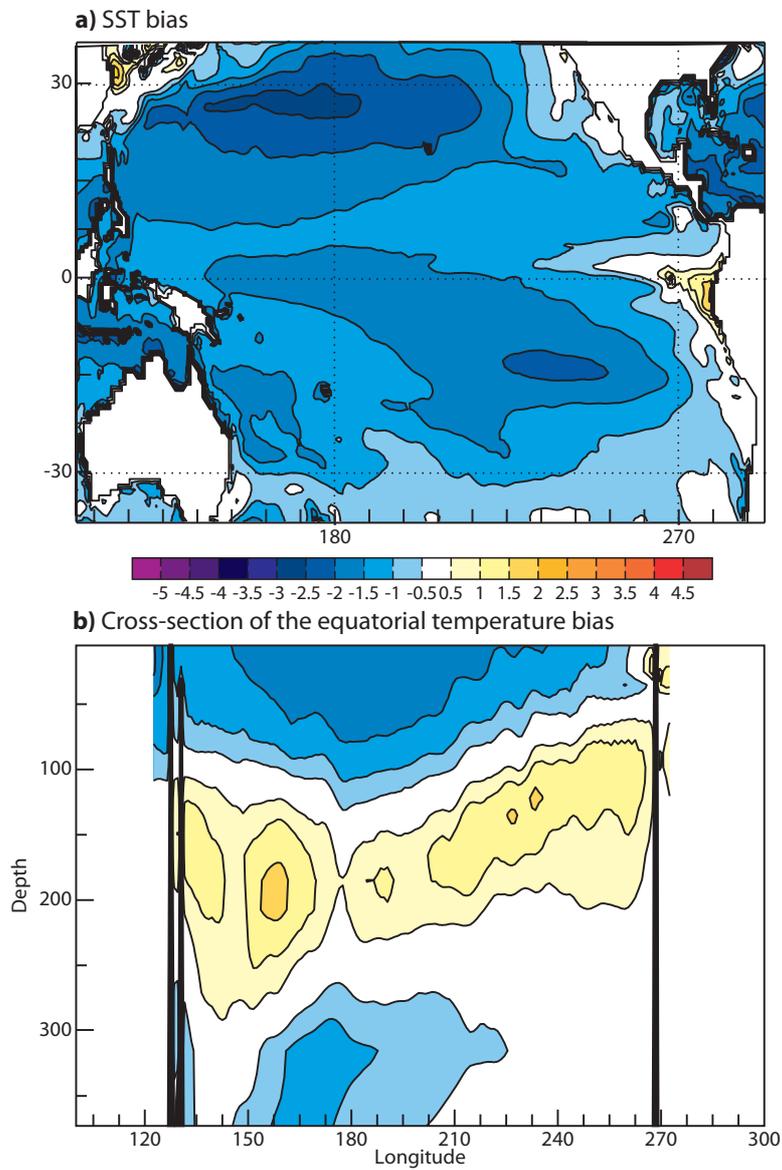
a) SST bias

b) Cross-section of the equatorial temperature bias

Figure 7: Difference between the Ucorr forecast and the reanalysis for forecast year 3-10 (initial date November 1980).

a) SST bias

b) Cross-section of the equatorial temperature bias
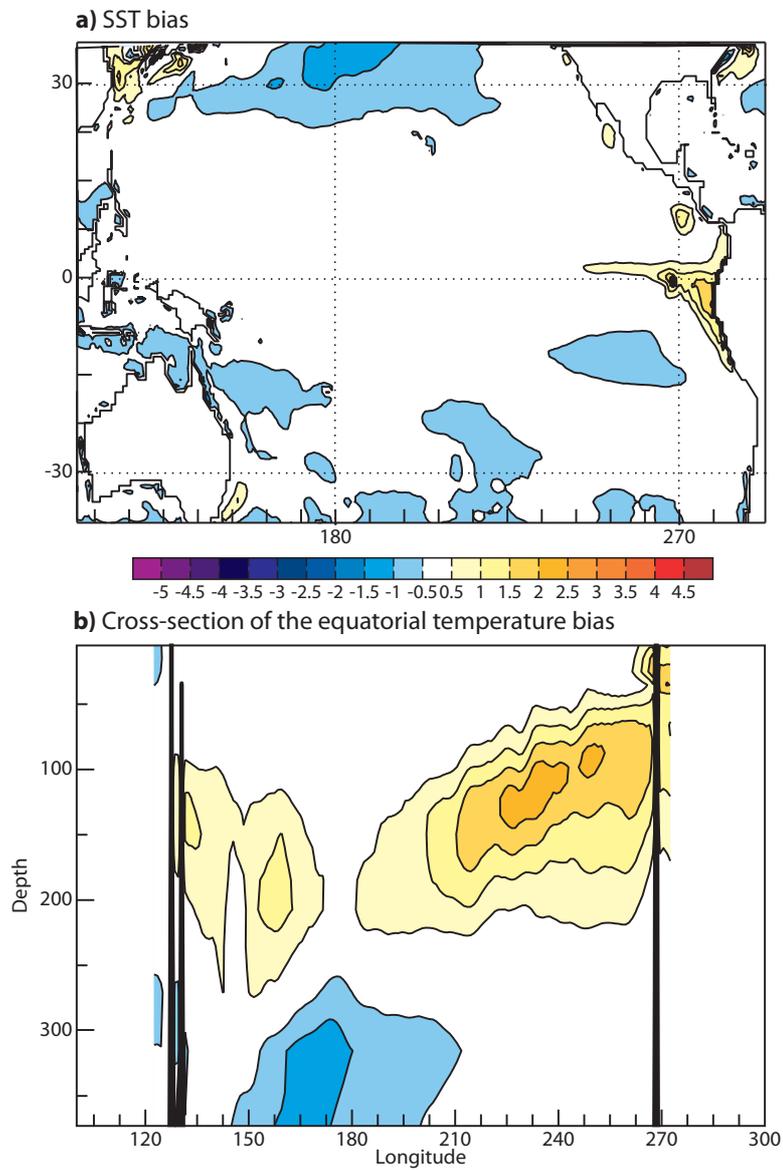

Figure 8: Difference between the UHcorr forecast and the reanalysis for forecast year 3-10 (initial date November 1980).
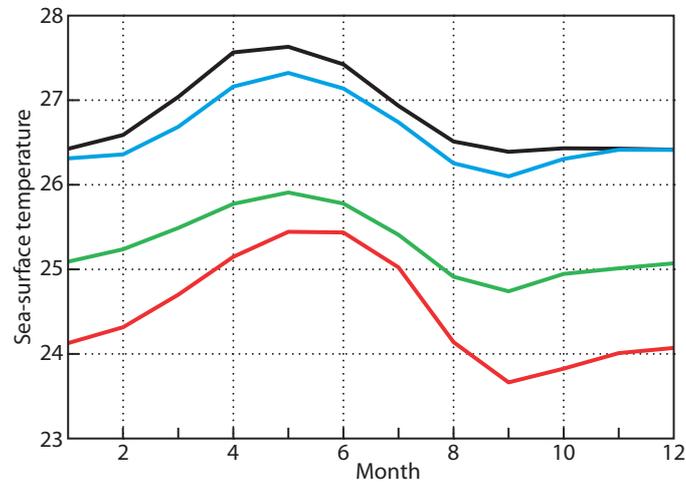
Figure 9: Monthly mean SST for Niño3.4. Reanalysis (black), NOcorr (red), Ucorr (green) and UHcorr (blue).
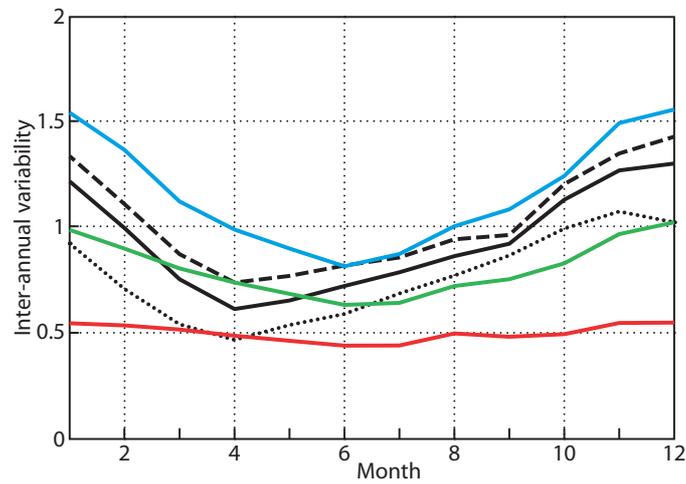

Figure 10: SST standard deviation for Niño3.4 as a function of calendar month (seasonal cycle removed). Reanalysis 1970-2010 (black, solid), 1970-1980 (black, dotted) and 1990-2000 (black, dashed). NOcorr (red), Ucorr (green) and UHcorr (blue).
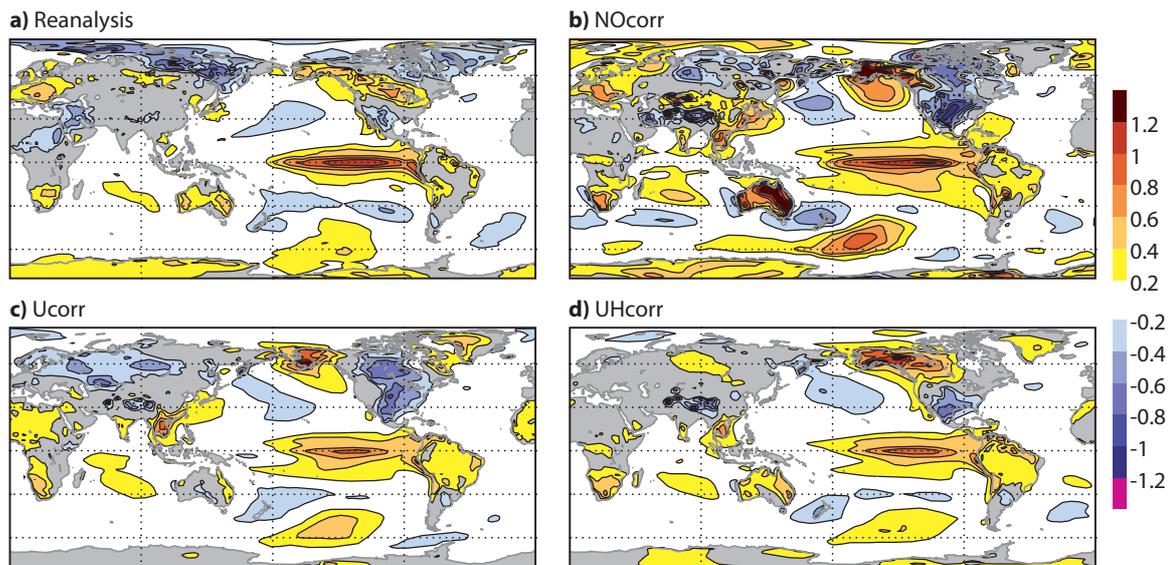
Figure 11: Regression of Niño3.4 SST to 2-metre temperature for DJF. The forecasts using forecast year 4-9 for the forecast initialised 1975 to 2000 and ERA Interim year 1979-2009.

Another important aspect of the ENSO variability is the seasonal phase locking of the SST variability (Misra et al., 2007). One of the characteristics is that the ENSO events peak at the end of the calendar year. Here we see that the reanalysis has the highest variability in December as expected and the lowest in April. For the Ucorr experiment, the results are similar, but the level for the variability is in better agreement with the reanalysis. The results for the NOcorr experiment shows a low level of variability and only a tiny sign of phase locking of ENSO. This is a further sign of its inability to simulate ENSO in the NOcorr experiment.

For the UHcorr experiment, the phase locking maximum appears in December as it does in the reanalysis, while the minimum appears in June instead of April. One plausible explanation lies in the seasonality of the westerly wind burst (associated to large SST values), with the potential of triggering ENSO events: inspection of Figures 9 and 10 would suggest an approximately 3-month lag between the time of the maximum of SST and the minimum of variability. But understanding the reason for the shift of the minimum is beyond the scope of this study.

Comparing the reanalysis data for 1970-1980 (dotted lines) and 1990-2000 (dashed) we see a large difference in the variability; the 90's were a much more active period than the 70's. There has been some discussion in the literature about decadal differences in the ENSO variability, e.g Balmaseda et al. (1995) and Wang and Picaut (2004). The level of variability for the 1990-2000 is close to the one obtained for the UHcorr experiment, while a large difference is present between the observed in 1970-1980 and UHcorr. However, one should bear in mind the uncertainties in the observations especially before 1980, and therefore differences between the ENSO variability prior and after 1980 could partly be due to changes in the observing systems.

Figure 11 shows the linear regression of the Niño3.4 SST onto 2-metre temperature. This diagnostic gives a measure of the teleconnections from an ENSO event with a certain amplitude. It does not account for the differences in the ENSO amplitude and variability between the experiments. Compared with ERA Interim, the NOcorr experiment yields, in general, stronger teleconnections. However, we have to bear in mind that the amplitude of the ENSO events is only a half in the NOcorr experiment. Both NOcorr and Ucorr show a bad pattern over north-America, while UHcorr is in better agreement with the pattern
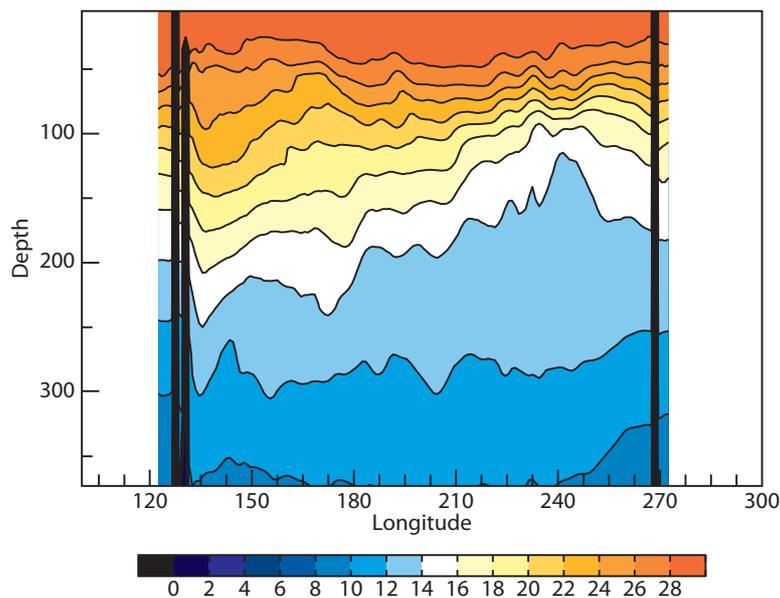
Figure 12: Vertical cross-section of the temperature along the equator in the Pacific for January 1998.

from the reanalysis.

4.3 Trajectories in a reduced phase-space

Figure 12 shows the vertical cross-section of the ocean temperature for the reanalysis along the equator for January 1998, during the end of a strong El Niño event. Compared to the climatological cross-section shown in Figure 5(b), a difference in the structure of the thermocline is present. The westward tilt of the thermocline is gone, as well as the horizontal gradient of the SST. The thermocline depth is shallower than normal. For the purpose of diagnostics, we reduce the ENSO dynamics to the three following degrees of freedom: the thermocline depth in the (1) eastern and (2) western basin together with (3) the SST in the Niño3.4 area. While the SST anomaly is the usual measure of the ENSO phase, the difference in the thermocline depth gives a measure of the tilt of the thermocline and the mean is a measure of the Equatorial upper ocean heat content. The phase space covered by the model (or reanalysis) could be approximated as an "ENSO attractor", i.e. the likely combination of the variable values. The concept of this diagnostic follows the ideas about recharge oscillator presented in Jin (1997a). The thermocline depth for the western Pacific is defined as the mean depth of the $20°C$ isoterm in ($140°E$-$170°W$, $5°N$-$5°S$) and for eastern part ($170°W$-$120°W$, $5°N$-$5°S$). The SST in Niño3.4 is defined as the mean over that region ($170°W$-$120°W$, $5°N$-$5°S$). The $20°C$ isoterm corresponds to the yellow colour in Figure 12 and Figure 5.

In Figure 13(a) the phase diagram is shown, with the SST of Niño3.4 on the y-axis and the average thermocline depth in the basin between ($140°E$-$120°W$) on the x-axis, using daily data. The figure shows the phase space trajectory for the reanalysis (red) between November 1995 and 2005 together with one member from the NOcorr ensemble (blue) and UHcorr (green). The brightness of the colour represents different time of the year where the darkest shade represents November and the white is around June/July. The forecast period and the forecast members are the same as highlighted in Figure 4 and plotted in Figure 14(d). The ensemble members used for this diagnostic are chosen because they have the strongest ENSO cycle for the November 1995 initialisation among the ensemble members (in 1997 for UHcorr
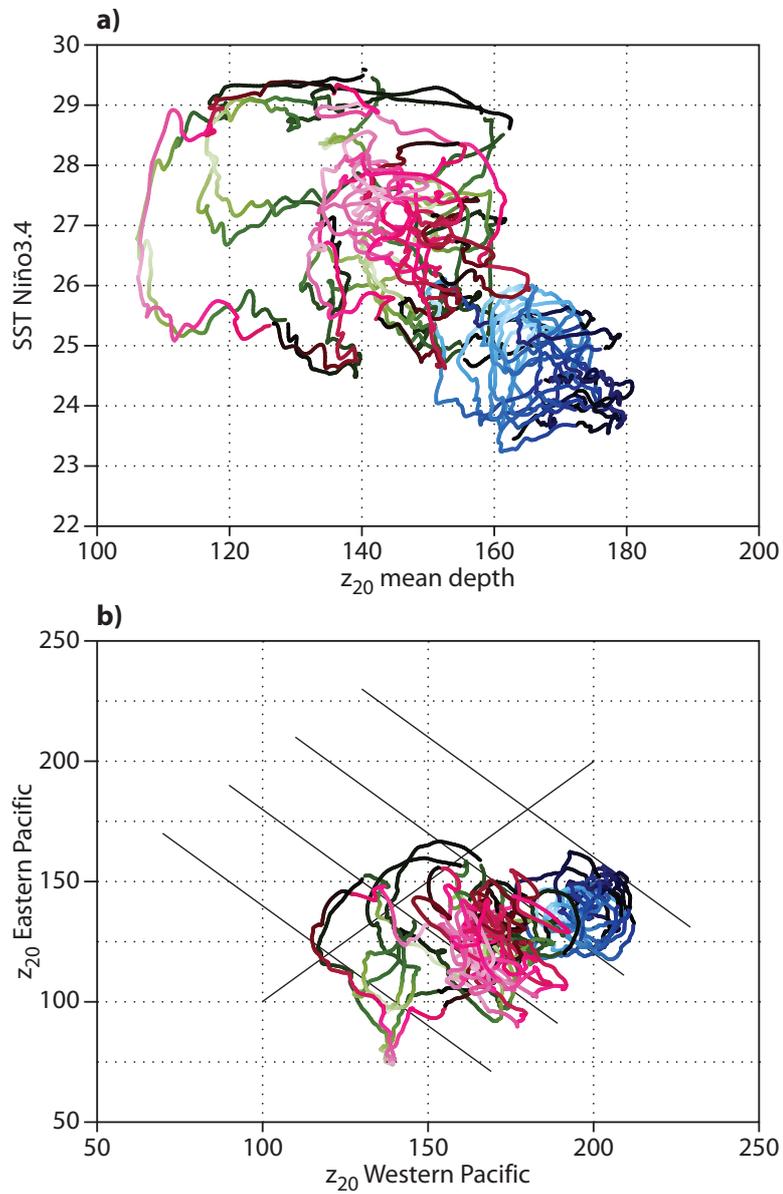
Figure 13: Phase space trajectories for reanalysis (red), NOcorr (blue) and UHcorr (green). Nov 1995 to Nov 2005. Black represent November and white is around June/July.

and in 2003 for NOcorr).

In the reanalysis, ENSO cycle appears as an anti-clockwise cycle. In the beginning of the cycle, the SST rises while the thermocline is deep. In the next process, the thermocline "discharges" heat while the SST is high. Suddenly, cold water starts to upwell and the SST decreases rapidly. Finally, the thermocline depth increases while the SST is low during the La Niña phase. This cycle is especially clear for the 1997-1998 event, which is the outermost loop of the reanalysis and January 1998 (as plotted in Figure 12) is almost in the upper corner with the highest SST and the close to the most shallow thermocline.

Comparing the UHcorr forecast (green) with the reanalysis, we see that the phase space of the both coincide. This indicates that the mean and the variability of the ENSO are similar. One should note that the SST forecast for this particular member in the Niño3.4 region is almost perfect [cf. Figure 14(d)]. However, the UHcorr forecast also shows two more El Niño events with similar structure to the 1997-1998 event (three periods are present with SSTs of around $27°$ Celsius), which is a sign of the over-activity discussed in the previous section. Regarding the NOcorr forecast, the phase space is shifted towards colder SST and deeper thermocline and the variability in the phase space is lower for the NOcorr forecast. One can also see a more regular behaviour of the trajectories in the phase-space, indicating that the stronger seasonal variability dominates over the inter-annual variability (the coldest SST and deepest thermocline always appear in December).

Figure 13(b) shows another dimension of the phase space, with the thermocline depth in the western part of the basin on the x-axis and eastern part on the y-axis. The mean depth is given by the average of the both parts and isolines for the mean depth is plotted for 120, 140, 160 and 180 metres [to be compared to Figure 13(a)]. The 1-1 line means no tilt of the thermocline and right of the line the tilt is towards west. During an El Niño, the thermocline change its tilt from westwards to neutral or even eastwards. [January 1998 for the reanalysis is located in the far left part of Figure 13(a) with a shallow thermocline, especially shallow in the western Pacific (x-axis in Figure 13(b)].

In terms of the NOcorr experiment, a strong tilt towards west is always present, which is maintained by the strong easterly winds. We also see that the deeper thermocline is mostly contributed to by the western part, where we have a strong warm sub-surface bias. For the UHcorr experiment the phase space is similar to the reanalysis. Also here we see a good agreement with the 1997/1998 ENSO event, but that two additional El Niño events are also visible as in Figure 13(a).

These diagnostics show that the flux correction not only impacts the mean SST but the whole of the ENSO dynamics. The strong easterly winds in the NOcorr experiment yield a strong thermocline tilt, and the simulations do not even approch obtaining a flat thermocline, which should appear for strong El Niño events.

4.4   Impact on the atmospheric variability

As described in Section 2, the Walker circulation is the atmospheric counter-part of the equatorial oceanic circulation in the tropical Pacific, driven by the convection in the western Pacific and over the Maritime Continent. It consists of easterly winds in the lower troposphere, rising motion in the western part of the basin (connected with negative pressure anomaly at sea-level), westerlies in the upper troposphere and sinking motion in the eastern part of the basin (connected with high sea-level pressure).

In order to investigate the vertical structure of the circulation and its variability, Howmöller diagrams have been plotted of the vertical cross-section of the zonal wind for the Niño3.4 area (Figure 14). In Figure 14(d) the corresponding time-series of the Niño3.4 SST with a 12-month running mean applied
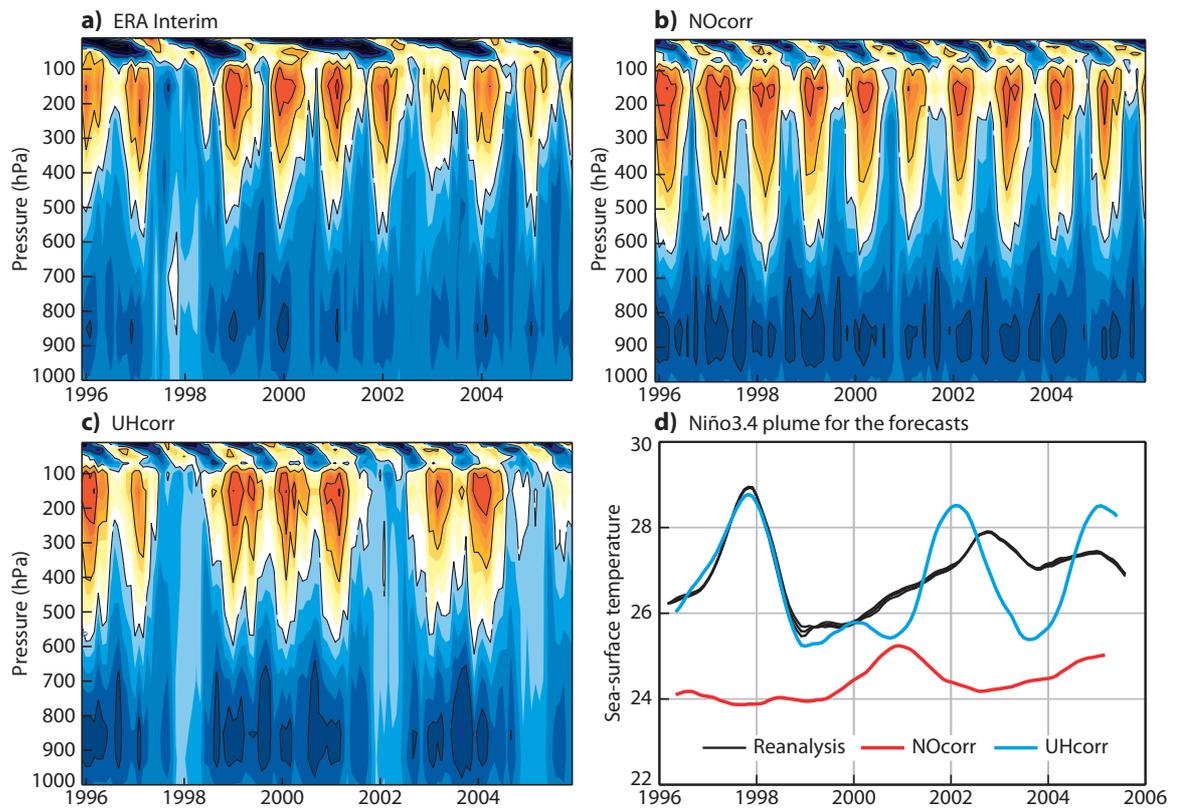
Figure 14: Vertical Howmöller diagram of zonal wind speed averaged for Niño3.4 area (westerlies-yellow, easterlies-blue). Contour interval 2.5 m/s.

is plotted, in order to compare the ENSO phase with the wind pattern. The UHcorr member (blue line) has the 1997/1998 ENSO event in phase with the reanalysis, although afterwards the forecast contains a higher ENSO variability compared to the reanalysis (as already discussed above). Regarding the NOcorr forecast we see one weak El Niño event in 2001, but otherwise the ENSO variability is low, as expected from the previous diagnostics.

Figure 14(a) shows a vertical Howmöller diagram of the zonal wind speed for the reanalysis (ERA Interim). In general, the easterlies (negative u-wind) dominate the lower troposphere and the westerlies dominate the upper part. For 1997-1998 [the years with a strong El Niño as seen in Figure 14(d)], we see that the circulation has broken down. From spring 1997 to the spring 1998 the easterlies are dominating the upper troposphere and for the some part of the lower troposphere the winds are westerly.

In Figure 14(b) we see the same Howmöller diagram for the same time period for the NOcorr forecast. Here we cannot see the inter-annual variability in the upper-tropospheric winds as for the El Niño event forecast in 2001 only a weak signal in the upper-tropospheric winds is visible.

Figure 14(c) shows the data from the the UHcorr forecast. This member forecasted strong El Niño events in 1998, 2002 and 2005 as seen in Figure 14(d). Studying the Howmöller diagram, we can clearly see these events in the wind pattern, in the same way as seen in the reanalysis. These results clearly show that the amplitude of the variability in the ocean and lower troposphere has an influence on the large-scale upper tropospheric wind pattern.

Figure 15(a) shows a histogram of the Southern Oscillation Index (SOI), based on monthly means for forecast years 3-10. The index is defined as the pressure difference between Easter Islands ($27°$S,$109°$W) and Darwin ($12°$S,$131°$E). A weak (strong) pressure gradient is the signature of El Niño (La Niña). The results show that the NOcorr forecast is biased towards a too high pressure gradient, looking like a constant La Niña. The distribution is too narrow compared to the reanalysis, indicating that the variability is too weak. For the Ucorr (green) experiment the distribution is shifted towards a weaker gradient and is closer to the reanalysis, although the mean of the gradient is still too strong. For the UHcorr experiment (blue), the distribution agrees well with the reanalysis, both in mean and in width. The over-activity seen in the SST is not so obvious here. However, the tail on the negative side (El Niño) is longer for the UHcorr experiment (although the tail is difficult to see in the figure).

For the development of El Niño events, the wind stress in the western part of the equatorial Pacific is important [discussed in e.g Vitart et al. (2003)]. The zonal wind stress affects the tilt of the thermocline; strong easterlies give a strong tilt to the thermocline (Jin, 1997a), while the westerly wind bursts (WWB) tend to reduce the tilt by deepening the thermocline in the Eastern Pacific, reducing the upwelling and producing a warming in the Eastern Pacific. This remote effect, together with a more local effect on the eastern displacement of the warm pool by zonal advection, can trigger the occurrence of ENSO events.

In order to investigate the appearance of such westerlies, the histogram of daily data for the zonal momentum flux has been plotted for the Niño4 area [Figure 15(b)]. This diagnostic includes the flux-correction on the wind stress. For the NOcorr experiment we see that there are no days in the 16 (last 8 years in the forecasts from 1985 and 1995) year period where the mean wind in the area is westerly. By applying the momentum-flux correction, the distribution is shifted towards more westerly wind. The shift is about 0.01 N/m^2 that corresponds well with the applied flux-correction [compared with Figure 3(a)]. The momentum-flux correction does not only induce a shift in the distribution of zonal wind stress, but it also broadens it, producing longer tails. The difference between Ucorr and UHcorr is small although the additional heat-flux correction broaden the distribution slightly (as an effect of the higher ENSO variability). For the UHcorr, the tail for westerlies is even longer than that of the reanalysis (more frequent westerlies in UHcorr than the reanalysis).
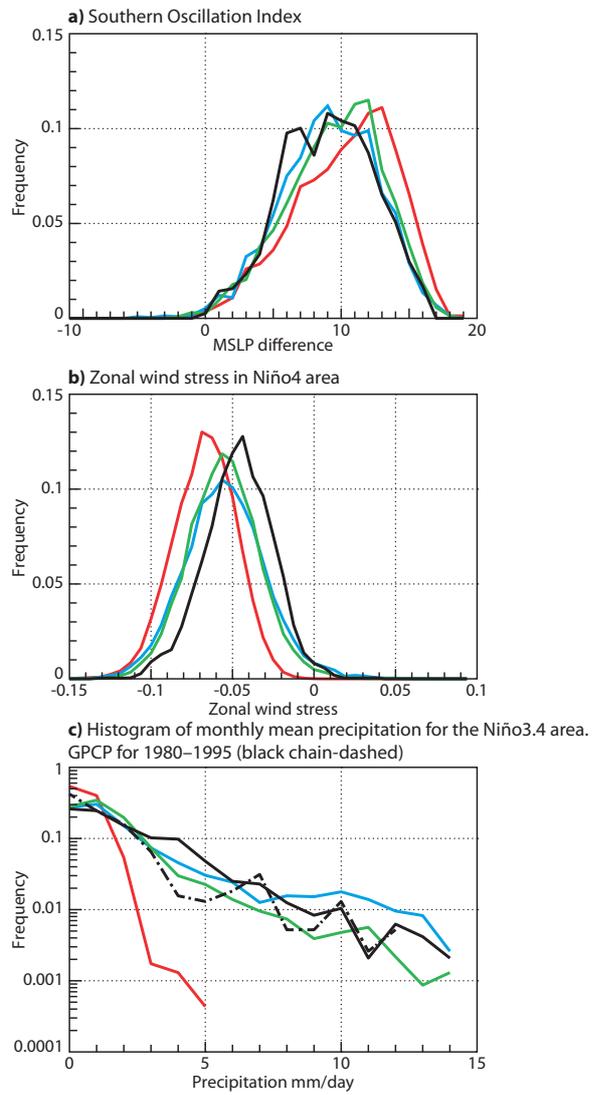
Figure 15: Histogram of ENSO statistics. Reanalysis (black), NOcorr (red), Ucorr (green) and UHcorr (blue).
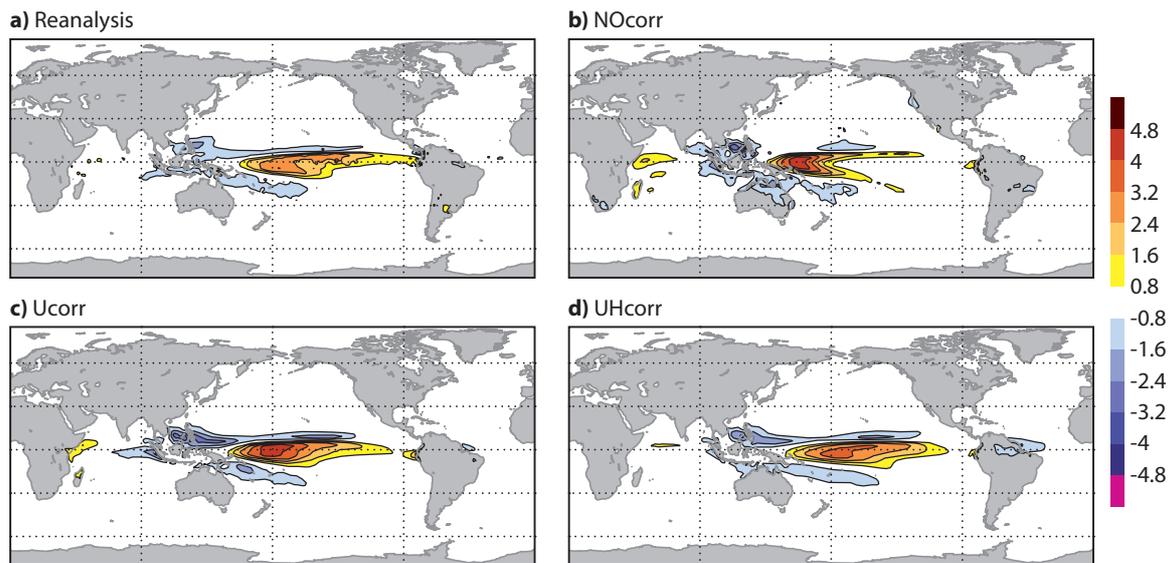
Figure 16: Regression of Niño3.4 SST to total precipitation for DJF. The forecasts using forecast year 4-9 for the forecast initialised 1975 to 2000 and ERA Interim year 1979-2009.

Figure 15(c) shows the histogram of the monthly precipitation rates for the Niño3.4 area for forecast years 3-10 with a logarithmic scale on the y-axis. During El Niño, the convection in the western Pacific moves eastward and affect this area. The y-axis has a logarithmic scale so that the rare events with high precipitation are highlighted. Due to the uncertainties in the precipitation in the ERA Interim (black, solid), the precipitation from GPCP (black, dash-dotted) has also been plotted. The main difference between the reanalysis and GPCP is that the latter has more months with very low precipitation (less than 1 mm/day), while ERA Interim has more months with precipitation between 3-5 mm/day. The tails of the distributions agree well. Regarding the forecast experiments, the NOcorr has the worst results. For this experiment, the rain periods are clearly under-represented, due to the cold SST bias that suppress the convection and the fact that the forecasts have too few El Niño events.

The precipitation is much better represented in both flux-corrected experiments and the distributions agree well with both GPCP and ERA Interim. However, in the UHcorr experiment, the strong precipitation are too frequent. This is connected to the over-representation of strong El Niño in the forecasts.

Figure 16 shows the regression of the Niño3.4 SST on the total precipitation. Here we see the strongest connection, not supringingly, in the western tropical Pacific. As expected, in ERA Interim the centre of gravity for the precipitation moves eastwards during El Niño events (positive regression coefficient), with a maximum to the east of the date line. The pattern for UHcorr [Figure 16(d)] agrees well with the pattern for ERA Interim [Figure 16(a)]. For the NOcorr experiment [Figure 16(b)], the centre of gravity is far to the west of the date line, explaining why there is no strong precipitation events even during El Niño for the Niño3.4 area. The results for the Ucorr experiment [Figure 16(c)] are in between the other two experiments.

Altogether, the results in this section show that the impact of correcting the mean state in the ocean also feedbacks onto the inter-annual variability of the atmosphere.

5   Conclusions and discussion

In this study we have investigated the impact of the model mean state on the simulation of El Niño events. In the presence of systematic model error, the mean state and the variability of the model could differ from the observed mean state and variability. In this study we investigate the relationship between the mean state and the variability by comparing coupled-model simulations using the standard model configuration with simulations where we have attempted to remove the mean error in the sea-surface temperature by applying flux-correction.

The forecasting system used is the ECMWF IFS model coupled to the NEMO ocean model. The current model setup develops a cold bias on the seasonal time-scale, which is pronounced in the tropical Pacific due to a strong upwelling of cold water in the eastern part of the equatorial Pacific. The cold bias in the tropical Pacific is connected to a bias in the zonal wind (strong easterly winds). The wind bias leads to a strong tilt in the thermocline and produces a very stable La Niña like state with cold SST, with weak inter-annual variability. It is shown that a part of the wind bias is present in model runs with strong constrain to observed SST, suggesting that the origins of the wind bias in is in the atmospheric model, and that the bias is enhanced in the coupled system by a positive feedback mechanism.

We have used flux-correction in order to change the model climate towards the observed mean state. A set of decadal coupled integrations have been conducted using three different strategies. One strategy only uses momentum-flux correction and another uses both momentum and heat-flux correction. In the third strategy model mean state is left uncorrected, and the integrations have been initialised using anomaly initialisation. An alternative approach could have been to use full initialisation strategy, as is currently used in seasonal forecasting, with a model drift in the first months into the integrations. However, the results for full initialisation and anomaly initialisation regarding the variability should be similar after the model has drifted to its climatology.

Results show that by applying momentum-flux correction it is possible to remove a part of the cold bias in the tropical Pacific. This result shows the importance of having the correct winds in order to obtain the correct SST mean state. With the combination of heat and momentum-flux correction most of the bias is removed, and this is the first test for a successful flux-correction.

Results also show that the mean state has a strong influence of the amplitude of the inter-annual variability. For the simulations with the cold bias present, hardly any strong El Niño events are simulated. By using momentum-flux correction, the inter-annual variability in the Niño3.4 SST is increased, and using both heat and momentum-flux correction strong El Niños and La Niñas appear. However, for the heat and momentum flux corrected experiment, the inter-annual variability seems to be too large compared to observed variability and for some ensemble members the oscillation seems to be regular, with an ENSO period length of 3 years. This is not the case for all forecasts, but is seems like several ENSO cycles with high amplitude appear after each other. The issue with perpetual ENSO is not new and is discussed e.g. in Misra et al. (2007). The reason for these multiple ENSO-cycles may lay in a too strong subsurface wave dynamics, as discussed in Jin (1997b). This could also explain the different phase locking to the seasonal cycle as shown in Figure 10.

The increased variability in SST has also a strong influence on the atmospheric variability, for example in the impact on the Walker Circulation variability. The use of flux-correction also has a large affect on the precipitation amounts in the tropical Pacific. By correcting for the cold SST, the precipitation increases and the variability pattern shows more similarities with observed precipitation. Also teleconnections to other regions around the Pacific are better simulated with the corrected mean state.

The variability is not only important for the simulations of the ENSO events but also create a suffi-

cient ensemble spread. If the model variability is too low the ensemble spread will be low as well (Bengtsson et al., 2008) and the ensemble becomes over-confident.

These results are important for the choice of forecast strategies for seasonal and decadal forecasts. This study shows that the biased mean state severely affects the ENSO variability and teleconnections. By applying anomaly initialisation, the systematic errors are already present in the initial conditions of the forecast, and the errors in the variability will deteriorate results already in the early forecast ranges. If using full initialisation (initialised with the observed state), the model will eventually drift to its own climate. In this case there is the added difficulty that errors in the variability will change as a function of lead time, and in the case of strong nonlinearities, even the estimation of the bias (for a-posteriori bias correction) can be difficult. For the choice of forecast strategy, practical considerations in calculating the climatologies (applicable for anomaly initialisation), the correction required (flux correction) and time-dependent bias correction (full initialisation) are of importance. A companion paper discusses the forecast strategies in more detail, with focus on the forecast skill.

It may be possible that there is no such as thing as the best forcast strategy: different CGCMs have different biases, and a forecast strategy that works well for one model may be detrimental for another. In Spencer et al. (2007) the model had a cold SST bias in the equatorial Pacific and a too strong inter-annual variability, while the model in this study had a cold bias and too low inter-annual variability. In our study we have traced a large part of the bias in the equatorial Pacific to a wind bias, which makes the momentum-flux correction relevant, while the momentum-flux correction in Spencer et al. (2007) had a minor impact on the inter-annual variability.

The results in this study show that it is difficult to interpret results regarding a change in ENSO variability for future climate if the model itself is biased. A change in the ENSO activity could then either be due to climate change or a nonlinear effect of the systematic error in the model. However, in order to predict strong ENSO events, it is needed that the model could simulate such a amplitude of the variability. This study concludes that a correct mean state is needed to allow such a variability.

Acknowledgements

References

Balmaseda, M. A. and D. L. T. Anderson, 2009: Impact of initialization strategies and observations on seasonal forecast skill. *Geophys. Res. Lett.*, **36**, L1701.

Balmaseda, M. A., M. K. Davey, and D. L. T. Anderson, 1995: Decadal and Seasonal Dependence of ENSO Prediction Skill. *J. Climate*, **8**, 2705–2715.

Balmaseda, M. A., K. Mogensen, F. Molteni, and A. T. Weaver, 2010: The NEMOVAR-COMBINE ocean re-analysis. COMBINE Technical Report 1, FP7 COMBINE project.

Bengtsson, L. K., L. Magnusson, and E. Källén, 2008: Independent Estimations of the Asymptotic Variability in an Ensemble Forecast System. *Mon. Wea. Rev.*, **136**, 4105–4112.

Bjerknes, J., 1969: Atmospheric teleconnections from the equatorial Pacific. *Mon. Wea. Rev.*, **97**, 163–172.

Dee, D. P., et al., 2011: The ERA-Interim reanalysis: configuration and performance of the data assimilation system. *Q. J. R. Met. Soc.*, **137**, 553–597.

Eisenman, L., I. Yu and E. Tziperman, 2005: Westerly Wind Bursts: ENSO's Tail Rather than the Dog? *J. Climate*, **18**, 522–5238.

Guilyardi, E., 2006: El Nino-mean state-seasonal cycle interactions in a mutil-model ensemble. *Clim. Dyn.*, **26**, 329–248.

Guilyardi, E., A. Wittenberg, A. Fedorov, M. Collins, C. Wang, A. Capotondi, G. J. v. Oldenborgh, and T. Stockdale, 2009: Understanding El Nino in ocean-atmosphere general circulation models. *Bull. Amer. Meteor. Soc.*, **90**, 324–340.

Halpert, M. S. and C. F. Ropelewski, 1992: Surface Temperature Patterns Associated with the Southern Oscillation. *J. Climate*, **5**, 577–593.

Huffman, G. J., D. T. Adler, D. T. Bolvin, and G. Gu, 2009: Improving the global precipitation record: GPCP Version 2.1. *Geophys. Res. Lett.*, **36**, L17 808.

Jin, E. K., et al., 2008: Current status of ENSO prediction skill in coupled ocean-atmosphere models. *Clim. Dyn.*, **31**, 647–664.

Jin, F.-F., 1997a: An Equatorial Ocean Recharge Paradigm for ENSO. Part I: Conceptual Model. *J. Atm. Sci.*, **54**, 811–829.

Jin, F.-F., 1997b: An Equatorial Ocean Recharge Paradigm for ENSO. Part II: A Stripped-Down Coupled Model. *J. Atm. Sci.*, **54**, 830–847.

Keenlyside, N. S., M. Latif, J. Jungclaus, L. Kornblueh, and E. Roeckner, 2008: Advancing decadal-scale climate prediction in the North Atlantic sector. *Nature*, **453**, 84–88.

Kessler, W. S. and R. Kleeman, 2000: Rectification of the Madden-Julian oscillation into the ENSO cycle. *J. Climate*, **13**, 3560–3575.

Kirtman, B. P. and P. S. Schopf, 1998: Decadal variability in ENSO Predictability and Prediction. *J. Climate*, **11**, 2804–2822.

Lengaigne, M., E. Guilyardi, J. P. Boulanger, C. Menkes, P. Delecluse, P. Inness, J. Cole, and J. Slingo, 2004: Triggering of El Nino by westerly wind events in a coupled general circulation model. *Climate Dyn.*, **23**, 601–620.

Madec, G., 2008: NEMO reference manual, ocean dynamics component: NEMO-OPA. Note du Pole de Modelisation 27, Institut Pierre-Simon Laplace (IPSL), France.

Manganello, J. V. and B. Huang, 2009: The influence of systematic errors in the Southeast Pacific on ENSO variability and prediction in a coupled GCM. *Clim. Dyn.*, **32**, 1015–1034.

Misra, V., et al., 2007: Validating and understanding the ENSO simulation in two coupled climate models. *Tellus A*, **59**, 292–308.

Molteni, F., et al., 2011: The new ECMWF seasonal forecast system (System 4). Technical Memorandum 656, ECMWF.

Neelin, J. D. and H. A. Dijkstra, 1995: Ocean-Atmosphere Interaction and the Tropical Climatology. Part I: The Dangers of Flux Correction. *J. Climate*, **8**, 1325–1342.

Palmer, T., R. Buizza, F. Doblas-Reyes, T. Jung, M. Leutbecher, J. Shutts, G, M. Steinheimer, and A. Weisheimer, 2009: Stochastic parametrization and model uncertainty . Technical Memorandum 598, ECMWF.

Pierce, D. W., T. P. Barnett, R. Tokmakian, A. Semtner, M. Maltrud, J. Lysne, and A. Craig, 2004: The ACPI project, Element 1: Initializing a coupled climate model from observed conditions. *Climatic Change*, **62**, 13–28.

Reynolds, R. W., T. M. Rayner, D. C. Smith, D. C. Stokes, and W. Wang, 2002: An improved in situ and satellite SST analysis for climate. *J. Climate*, **15**, 1609–1625.

Ropelewski, C. F. and M. S. Halpert, 1987: Global and Regional Scale Precipitation Patterns Associated with the El Nino/Southern Oscillation. *Mon. Wea. Rev.*, **115**, 1606–1626.

Schneider, E. K., B. Huang, Z. Zhu, D. G. DeWitt, J. L. Kinter, B. P. Kirtman, and J. Shukla, 1999: Ocean Data Assimilation, Initialisation, and Predictions of ENSO with a Coupled GCM. *Mon. Wea. Rev.*, **127**, 1187–1207.

Smith, D., A. Cusack, A. Colman, C. Folland, and G. Harris, 2007: Improved surface temperature predictions for the coming decade from a global circulation model. *Science*, **317**, 796–799.

Spencer, H., R. Sutton, and J. M. Slingo, 2007: El Nino in a Coupled Climate Model: Sensitivity to Changes in Mean State Induced by Heat Flux and Wind Stress Corrections. *J. Climate*, **20**, 2273–2298.

Suarez, M. and P. S. Schopf, 1988: A Delayed Action Oscillator for ENSO. *J. Atm. Sci.*, **42**, 3283–3287.

Uppala, S. M., et al., 2005: The ERA-40 re-analysis. *Quarterly Journal of the Royal Meteorological Society*, **131**, 2961–3012.

Vitart, F., M. A. Balmaseda, L. Ferranti, and D. L. T. Anderson, 2003: Westerly wind events and the 1997/1998 El Nino event in the ECMWF Seasonal Forecasting System: A case study. *J. Climate*, **16**, 3153–3170.

Walker, G. T., 1924: Correlation in seasonal variations of weather, IX: A further study of world weather. *Mem. Indian Meteor. Dept.*, **24**, 275–332.

Wang, C. and J. Picaut, 2004: Understanding ENSO Physics - A Review. *Earth's climate: The ocean-Atmosphere Interaction, Geophysical Monograph series, Volume 147, AGU, Washington D. C.*